

# Tissue mechanics modulate microRNA-dependent PTEN expression to regulate malignant progression

Janna K Mouw<sup>1</sup>, Yoshihiro Yui<sup>1</sup>, Laura Damiano<sup>1</sup>, Russell O Bainer<sup>1</sup>, Johnathon N Lakins<sup>1</sup>, Irene Acerbi<sup>1</sup>, Guanqing Ou<sup>1</sup>, Amanda C Wijekoon<sup>1</sup>, Kandice R Levental<sup>2</sup>, Penney M Gilbert<sup>3</sup>, E Shelley Hwang<sup>4</sup>, Yunn-Yi Chen<sup>5</sup> & Valerie M Weaver<sup>1,6–8</sup>

Tissue mechanics regulate development and homeostasis and are consistently modified in tumor progression. Nevertheless, the fundamental molecular mechanisms through which altered mechanics regulate tissue behavior and the clinical relevance of these changes remain unclear. We demonstrate that increased matrix stiffness modulates microRNA expression to drive tumor progression through integrin activation of  $\beta$ -catenin and MYC. Specifically, in human and mouse tissue, increased matrix stiffness induced miR-18a to reduce levels of the tumor suppressor phosphatase and tensin homolog (PTEN), both directly and indirectly by decreasing levels of homeobox A9 (HOXA9). Clinically, extracellular matrix stiffness correlated directly and significantly with miR-18a expression in human breast tumor biopsies. miR-18a expression was highest in basal-like breast cancers in which PTEN and HOXA9 levels were lowest, and high miR-18a expression predicted poor prognosis in patients with luminal breast cancers. Our findings identify a mechanically regulated microRNA circuit that can promote malignancy and suggest potential prognostic roles for HOXA9 and miR-18a levels in stratifying patients with luminal breast cancers.

Tumors exhibit altered tissue-level and cell mechanics, including extracellular matrix (ECM) remodeling and stiffening, elevated interstitial pressure and altered mass transport<sup>1</sup>. Experimental models demonstrate that enhancing ECM stiffness promotes malignancy and, conversely, inhibiting matrix stiffening reduces tumor incidence and improves treatment<sup>2–4</sup>. Nevertheless, the molecular mechanisms by which mechanics influence cell behavior to modulate malignancy are poorly understood. Additionally, the clinical consequences of altered biophysical cues in the onset, histopathology and progression of cancer remain unclear.

MicroRNAs (miRNAs) are post-transcriptional regulators of gene expression that are altered in multiple cancers, where they modulate levels of tumor suppressors and oncogenes that regulate cell growth, survival and invasion<sup>5,6</sup>. miRNAs also regulate cell-cell and cell-matrix interactions, including integrin-dependent adhesion<sup>7</sup>. Integrin signaling is increased in tumors and reduced when ECM stiffening is prevented, indicating potential functional links between miRNAs and tumor mechanics<sup>2,3</sup>. Indeed, ECM stiffness potentiates transforming growth factor- $\beta$ -induced miRNA-dependent metastasis of malignant mammary epithelial cells (MECs)<sup>8</sup>, and shear stress and cyclic stretch induce miRNAs in alveolar epithelial and endothelial cells<sup>9,10</sup>. These results indicate that miRNAs are sensitive to mechanical cues.

At the intersection of many pathways involved in malignant transformation is phosphoinositide 3-kinase (PI3K), which is critical for cell growth, survival and invasion<sup>11</sup>. We showed previously that ECM stiffness directly modulates ErbB receptor-dependent PI3K activation and MEC invasion and that PI3K signaling is reduced by inhibiting ECM stiffening *in vivo*<sup>2,3</sup>, which implies that molecules that influence PI3K signaling are mechanically regulated. As a key negative regulator of PI3K activity, PTEN is a tumor suppressor whose expression is frequently reduced in human cancers<sup>12,13</sup>. Here, we used global profiling to identify a mechanically regulated miRNA, miR-18a, that targets PTEN, both directly and indirectly by decreasing levels of HOXA9, to promote PI3K-dependent malignancy. Clinically, miR-18a expression predicted clinical outcome in patients with luminal breast cancers.

## RESULTS

### ECM stiffness modulates miRNA expression

To identify molecular mechanisms whereby mammary tissue responds to differences in the mechanical microenvironment, we profiled miRNAs expressed in nonmalignant MCF-10A human MECs (hMECs) on soft (<400 Pa) or stiff (>5 kPa) polyacrylamide (PA) gels conjugated with recombinant basement membrane (Fig. 1a and Supplementary Tables 1 and 2). Interrogation of differentially

<sup>1</sup>Center for Bioengineering and Tissue Regeneration, Department of Surgery, University of California San Francisco (UCSF), San Francisco, California, USA.

<sup>2</sup>Department of Integrative Biology and Pharmacology, The University of Texas Health Science Center at Houston–Medical School, Houston, Texas, USA. <sup>3</sup>Institute of Biomaterials and Biomedical Engineering, University of Toronto, Toronto, Ontario, Canada. <sup>4</sup>Department of Surgery, Duke University Comprehensive Cancer Center, Durham, North Carolina, USA. <sup>5</sup>Department of Pathology, UCSF, San Francisco, California, USA. <sup>6</sup>Department of Anatomy and Department of Bioengineering and Therapeutic Sciences, UCSF, San Francisco, California, USA. <sup>7</sup>Eli and Edythe Broad Center of Regeneration Medicine and Stem Cell Research, UCSF, San Francisco, California, USA. <sup>8</sup>UCSF Helen Diller Comprehensive Cancer Center, UCSF, San Francisco, California, USA. Correspondence should be addressed to V.M.W. (valerie.weaver@ucsfmedctr.org).

Received 30 July 2013; accepted 10 February 2014; published online 16 March 2014; doi:10.1038/nm.3497

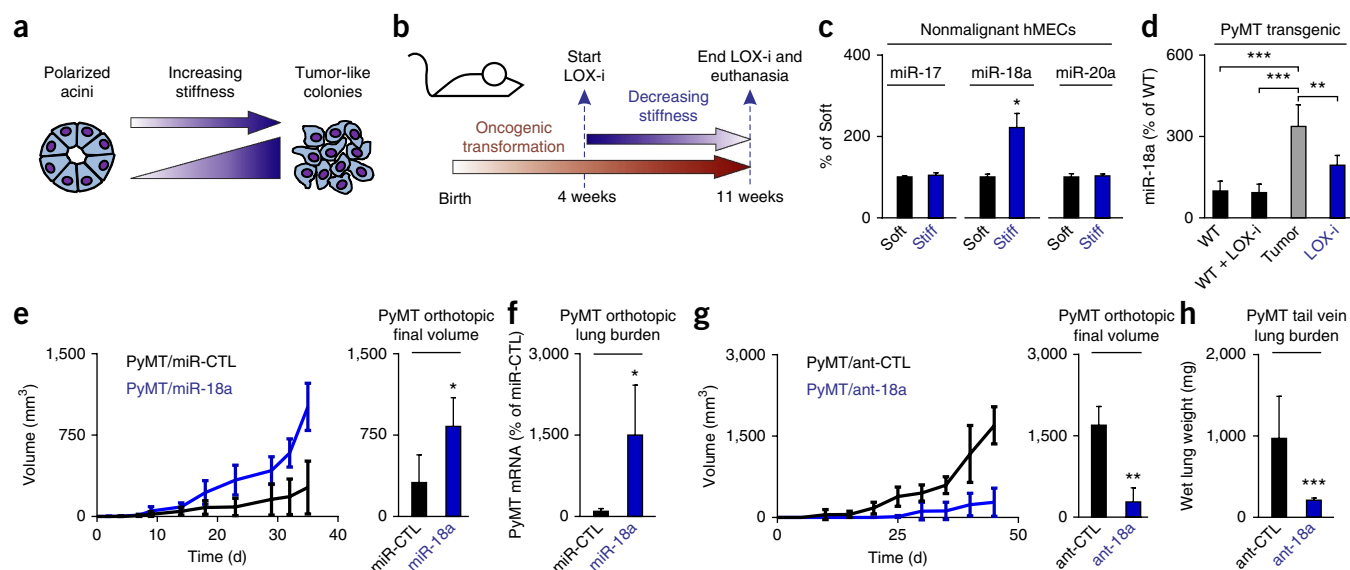


**Figure 1** ECM stiffness modulates miRNA expression in culture and *in vivo*. **(a)** Graphic depicting the *in vitro* experimental approach using hMECs and synthetic PA substrates functionalized with recombinant basement membrane to mimic the mechanical properties of the normal human mammary gland and of mammary tumors during malignant progression. **(b)** Graphic depicting the *in vivo* experimental approach inhibiting LOX (LOX-i) using the PyMT mouse model of breast cancer. **(c)** Validation and quantification of miR-17-92 targets (with  $P < 0.05$  from the microarray results) with quantitative PCR (qPCR). miRNA targets were normalized with RNU48 and graphed relative to the group cultured on PA gel <400 Pa (Soft). Stiff, group cultured on >5 kPa PA gel. **(d)** qPCR of miR-18a for FVB mice (WT), FVB mice treated with a LOX inhibitor (WT + LOX-i), control PyMT mice (Tumor) and PyMT mice treated with a LOX inhibitor (LOX-i,  $n = 10$  per group). Mouse miR targets were normalized with U6 and graphed relative to the FVB (WT) group. **(e)** Quantification of tumor growth and final tumor volume for PyMT primary tumor cells orthotopically injected into the inguinal mammary gland of FVB hosts ( $n = 6$  per group). PyMT cells expressed either a control construct (miR-CTL) or miR-18a. **(f)** Quantification of PyMT mRNA expression from the lungs of host FVB mice orthotopically injected with PyMT cells expressing either a control construct (miR-CTL) or miR-18a ( $n = 6$  per group). Results were normalized to 18S and graphed relative to miR-CTL. **(g)** Quantification of tumor growth and final tumor volume for PyMT primary tumor cells orthotopically injected into the inguinal mammary gland of FVB hosts ( $n = 5$  per group). PyMT cells expressed either a control antagomir (ant-CTL) or an antagomir to miR-18a (ant-18a). **(h)** Quantification of lung weight for FVB mice injected via tail vein with PyMT primary cells expressing either ant-CTL or ant-18a ( $n = 6$  per group). For *in vitro* bar graphs, results are the mean  $\pm$  s.e.m. of at least 3 independent experiments. For *in vivo* bar graphs, results are the mean  $\pm$  s.d. (\* $P < 0.05$ ; \*\* $P < 0.01$ ; \*\*\* $P < 0.001$ ).

expressed miRNAs showed changes in levels of total and mature miRNAs in response to stiffness and revealed that unprocessed miRNAs were somewhat disproportionately upregulated by ECM stiffness (two-sided Kolmogorov-Smirnov test,  $P = 0.040$ , **Supplementary Fig. 1a**). *In vivo*, in the polyoma middle T (PyMT) mouse model of breast cancer, we also observed that miRNAs were similarly regulated by ECM stiffness when we prevented ECM cross-linking and stiffening in mammary tumors by treating mice either with the lysyl oxidase (LOX) pharmacological inhibitor  $\beta$ -aminopropionitrile or with a specific function-blocking antibody to LOX; these results indicate that cellular miRNAs are responsive to matrix mechanics (**Fig. 1b** and **Supplementary Tables 3** and **4**).

We noted that within the pool of differentially expressed mature miRNAs in the hMECs cultured on the stiff PA gels, miRNAs belonging to the polycistronic miR-17-92 cluster were consistently induced (**Supplementary Table 1**). As the miR-17-92 cluster has been implicated in malignancy<sup>14,15</sup>, we explored the impact of this cluster on stiffness-mediated malignant transformation. Dysregulated expression of the cluster's individual miRNAs can drive malignancy through an imbalance of proliferation, apoptosis and differentiation<sup>15,16</sup>. Notably, only one specific cluster member, miR-18a, had significantly and consistently increased expression in response to ECM stiffness (**Fig. 1c**). Indeed, whereas the miR-17-92 cluster was upregulated with mouse mammary gland transformation, only miR-18a was significantly inhibited in PyMT tumors when tissue fibrosis and stiffening were reduced through LOX inhibition (**Fig. 1d** and **Supplementary**

**Fig. 2a–c**). As we were interested in identifying stiffness-regulated tumor suppressor pathways, we focused our efforts on delineating the role of miR-18a in the mechanical regulation of malignancy.

We first determined that substrate mechanics robustly and consistently increased miR-18a levels in several nonmalignant and transformed breast cancer cell lines<sup>17</sup> in culture (**Supplementary Fig. 1b**). We then confirmed that miR-18a induced no detectable changes in cell proliferation or apoptosis but did increase anchorage-independent colony formation in MCF-10A, MCF-7 and T4-2 breast cancer cells (**Supplementary Fig. 1c,d**). Orthotopic experiments conducted using PyMT mammary tumor cells injected into the cleared mammary fat pads of FVB mouse hosts revealed that increasing miR-18a levels enhanced growth and final tumor volume, as well as lung metastasis (**Fig. 1e,f**). We also found that antisense miRNA (antagomir)-mediated knockdown of miR-18a (ref. 18) in MCF-7 and T4-2 cells compromised their growth and survival in soft agar culture (**Supplementary Fig. 1e**). Indeed, knockdown of miR-18a reduced growth and final tumor volume of PyMT mammary tumor cells injected into the cleared fat pad of FVB mice (**Fig. 1g**) and inhibited their ability to form lung metastasis in a tail vein assay (**Fig. 1h** and **Supplementary Fig. 1f**). These findings identify miR-18a as a mechanically regulated tumor enhancer.

#### ECM stiffness induces miR-18a to reduce PTEN levels

We identified putative binding regions<sup>19–22</sup> for miR-18a in the 3' untranslated region (UTR) of the tumor suppressor PTEN

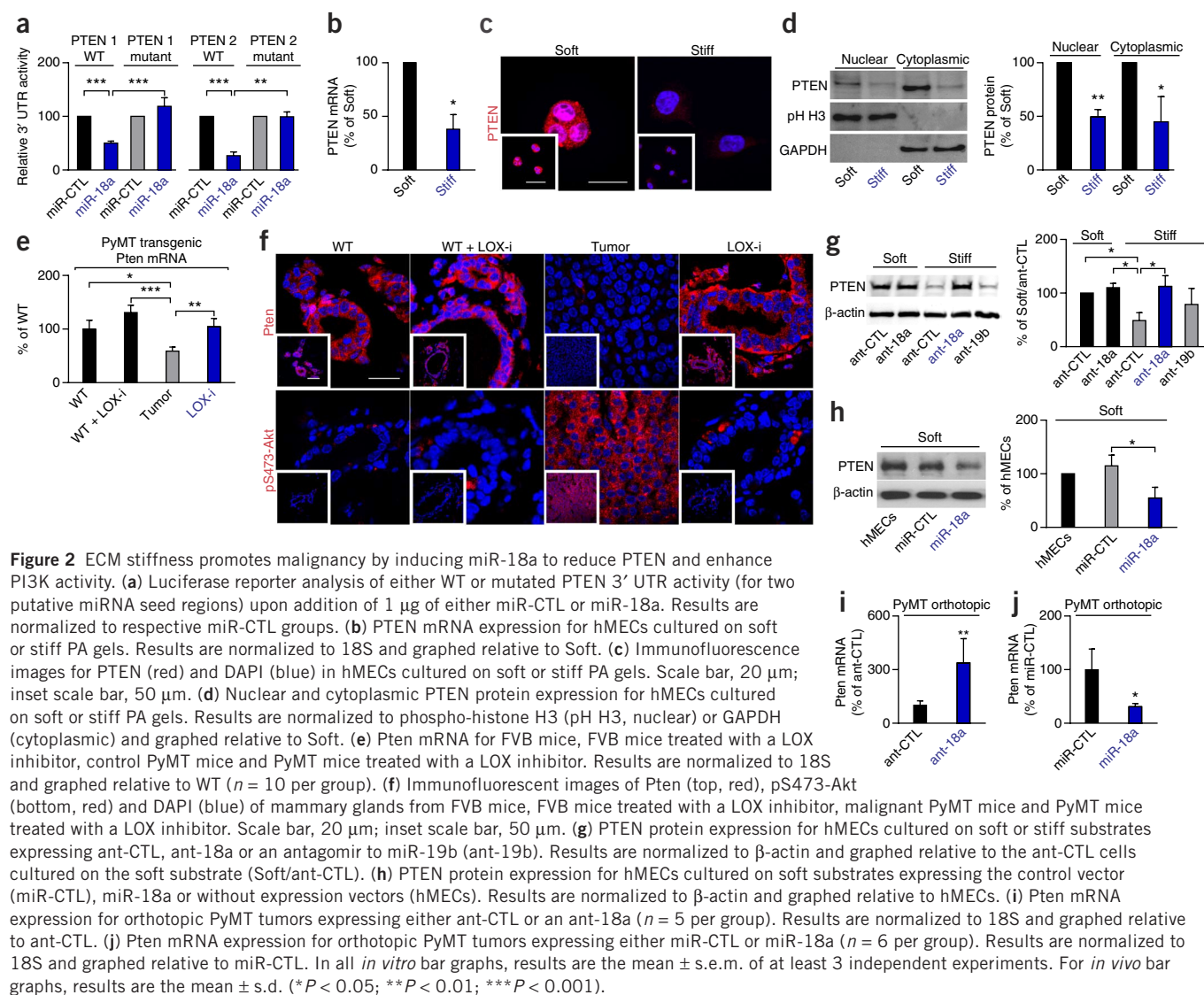


**Figure 2** ECM stiffness promotes malignancy by inducing miR-18a to reduce PTEN and enhance PI3K activity. (a) Luciferase reporter analysis of either WT or mutated PTEN 3' UTR activity (for two putative miRNA seed regions) upon addition of 1  $\mu$ g of either miR-CTL or miR-18a. Results are normalized to respective miR-CTL groups. (b) PTEN mRNA expression for hMECs cultured on soft or stiff PA gels. Results are normalized to 18S and graphed relative to Soft. (c) Immunofluorescence images for PTEN (red) and DAPI (blue) in hMECs cultured on soft or stiff PA gels. Scale bar, 20  $\mu$ m; inset scale bar, 50  $\mu$ m. (d) Nuclear and cytoplasmic PTEN protein expression for hMECs cultured on soft or stiff PA gels. Results are normalized to phospho-histone H3 (pH H3, nuclear) or GAPDH (cytoplasmic) and graphed relative to Soft. (e) Pten mRNA for FVB mice, FVB mice treated with a LOX inhibitor, control PyMT mice and PyMT mice treated with a LOX inhibitor. Results are normalized to 18S and graphed relative to WT ( $n = 10$  per group). (f) Immunofluorescent images of Pten (top, red), pS473-Akt (bottom, red) and DAPI (blue) of mammary glands from FVB mice, FVB mice treated with a LOX inhibitor, malignant PyMT mice and PyMT mice treated with a LOX inhibitor. Scale bar, 20  $\mu$ m; inset scale bar, 50  $\mu$ m. (g) PTEN protein expression for hMECs cultured on soft or stiff substrates expressing ant-CTL, ant-18a or an antagomir to miR-19b (ant-19b). Results are normalized to  $\beta$ -actin and graphed relative to the ant-CTL cells cultured on the soft substrate (Soft/ant-CTL). (h) PTEN protein expression for hMECs cultured on soft substrates expressing the control vector (miR-CTL), miR-18a or without expression vectors (hMECs). Results are normalized to  $\beta$ -actin and graphed relative to hMECs. (i) Pten mRNA expression for orthotopic PyMT tumors expressing either ant-CTL or an ant-18a ( $n = 5$  per group). Results are normalized to 18S and graphed relative to ant-CTL. (j) Pten mRNA expression for orthotopic PyMT tumors expressing either miR-CTL or miR-18a ( $n = 6$  per group). Results are normalized to 18S and graphed relative to miR-CTL. In all *in vitro* bar graphs, results are the mean  $\pm$  s.e.m. of at least 3 independent experiments. For *in vivo* bar graphs, results are the mean  $\pm$  s.d. (\* $P < 0.05$ ; \*\* $P < 0.01$ ; \*\*\* $P < 0.001$ ).

(Supplementary Fig. 3a). Reporter assays<sup>23</sup> using the putative wild-type (WT) and mutated 3' UTRs of PTEN confirmed that miR-18a interacts with and inhibits PTEN transcription at two of three predicted sites (Fig. 2a and Supplementary Fig. 3b). PTEN mRNA expression was reduced in hMECs grown on a stiff substrate (Fig. 2b). Immunofluorescence and immunoblotting also demonstrated loss of PTEN expression in hMECs grown on a stiff substrate, with markedly reduced expression in both the nuclear and cytoplasmic fractions (Fig. 2c,d). PTEN mRNA expression was similarly reduced in stiff mouse mammary tumor tissue, and inhibiting stromal stiffening prevented PTEN loss (Fig. 2e and Supplementary Fig. 2d). Finally, we documented an inverse correlation between PI3K activity, indicated by elevated levels of phosphorylated Akt on Ser473 (pS473-Akt), and PTEN protein, without any change in cell proliferation or apoptosis, which suggests that ECM stiffness could induce miR-18a to modulate malignant progression of the mammary gland by regulating PTEN (Fig. 2f and Supplementary Fig. 2e–g).

To directly implicate miR-18a in PTEN modulation, we tested whether antagomir-mediated knockdown of miR-18a could restore PTEN levels in hMECs grown on a stiff ECM. hMECs expressing an antagomir to miR-18a retained PTEN expression even when grown

on a stiff PA gel, in contrast to the modest increase observed in hMECs expressing an antagomir to miR-19b (Fig. 2g). PTEN levels were reduced when miR-18a was ectopically expressed in hMECs cultured on a soft ECM (Fig. 2h). Notably, PTEN mRNA expression was increased in PyMT tumors in which miR-18a levels had been reduced, and we noted a reduction in PTEN mRNA expression in PyMT tumors in which miR-18a levels had been increased (Fig. 2i,j). These findings demonstrate that ECM stiffness represses PTEN and promotes PI3K-dependent malignant progression of the mammary gland by increasing miR-18a levels.

### ECM stiffness induces miR-18a to reduce HOXA9 levels

miRNAs typically have multiple targets, and miRNA target prediction software<sup>19–22</sup> also identified a putative binding region for miR-18a in the 3' UTR of the homeobox transcription regulator HOXA9 (Supplementary Fig. 3a). We previously reported that HOXA9 restricts the malignant behavior of breast cancer cells *in vitro* and *in vivo* and that HOXA9 levels are reduced in human breast cancers and predict poor patient outcome<sup>24</sup>. Accordingly, we explored the impact of miR-18a on HOXA9.

Reporter assays using a 3' UTR of HOXA9 containing the putative miR-18a binding region confirmed that miR-18a interacts with and

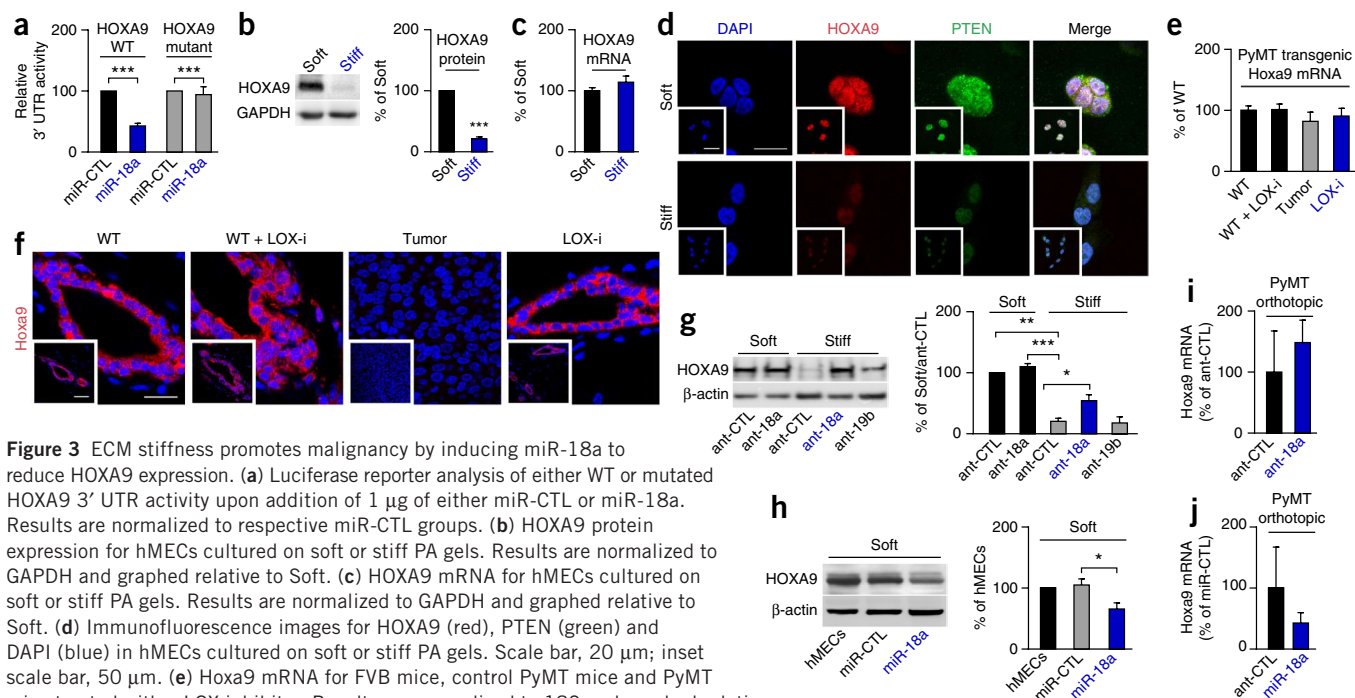


**Figure 3** ECM stiffness promotes malignancy by inducing miR-18a to reduce HOXA9 expression. (a) Luciferase reporter analysis of either WT or mutated HOXA9 3' UTR activity upon addition of 1  $\mu$ g of either miR-CTL or miR-18a. Results are normalized to respective miR-CTL groups. (b) HOXA9 protein expression for hMECs cultured on soft or stiff PA gels. Results are normalized to GAPDH and graphed relative to Soft. (c) HOXA9 mRNA for hMECs cultured on soft or stiff PA gels. Results are normalized to GAPDH and graphed relative to Soft. (d) Immunofluorescence images for HOXA9 (red), PTEN (green) and DAPI (blue) in hMECs cultured on soft or stiff PA gels. Scale bar, 20  $\mu$ m; inset scale bar, 50  $\mu$ m. (e) Hoxa9 mRNA for FVB mice, control PyMT mice and PyMT mice treated with a LOX inhibitor. Results are normalized to 18S and graphed relative to WT ( $n = 10$  per group). (f) Immunofluorescence images of Hoxa9 (red) and DAPI (blue) for FVB mice, FVB mice treated with a LOX inhibitor, control PyMT mice and PyMT mice treated with a LOX inhibitor. Scale bar, 20  $\mu$ m; inset scale bar, 50  $\mu$ m. (g) HOXA9 protein for hMECs cultured on soft or stiff substrates expressing ant-CTL, ant-18a or ant-19b. Results are normalized to  $\beta$ -actin and graphed relative to Soft/ant-CTL. (h) HOXA9 protein for hMECs cultured on soft substrates expressing miR-CTL or miR-18a or without expression vectors (hMECs). Results are normalized to  $\beta$ -actin and graphed relative to hMECs. (i) Hoxa9 mRNA expression for orthotopic PyMT tumors expressing either ant-CTL or ant-18a ( $n = 5$  per group). Results are normalized to 18S and graphed relative to ant-CTL. (j) Hoxa9 mRNA expression for orthotopic PyMT tumors expressing either miR-CTL or miR-18a ( $n = 6$  per group). Results are normalized to 18S and graphed relative to miR-CTL. In all *in vitro* bar graphs, results are the mean  $\pm$  s.e.m. of at least 3 independent experiments. For *in vivo* bar graphs, results are the mean  $\pm$  s.d. (\* $P < 0.05$ ; \*\* $P < 0.01$ ; \*\*\* $P < 0.001$ ).

inhibits HOXA9 expression and showed that mutating this domain ablates this regulation (Fig. 3a). Immunoblotting demonstrated significant loss of HOXA9 protein expression in hMECs grown on a stiff substrate, with no change in HOXA9 mRNA levels (Fig. 3b,c). Immunofluorescence analysis showed robust co-staining of HOXA9 and PTEN only in hMECs grown on soft ECM and a concomitant loss of both proteins when hMECs were grown on a stiff ECM (Fig. 3d). Moreover, immunofluorescence staining of mammary tissues detected high levels of Hoxa9 in normal mouse mammary tissue and showed that, whereas this expression was lost in the stiffened mammary tumor tissue, inhibiting tissue stiffness tempered the loss of Hoxa9, with little effect on mRNA expression (Fig. 3e,f and Supplementary Fig. 2d,e). These data suggest that miR-18a could also regulate mammary malignancy by regulating HOXA9.

To directly implicate miR-18a in HOXA9 modulation, we tested whether antagonist-mediated knockdown of miR-18a could restore HOXA9 levels in hMECs grown on a stiff ECM. hMECs expressing an antagonist to miR-18a retained HOXA9 expression even when grown on a stiff PA gel (Fig. 3g). Moreover, HOXA9 levels were reduced when miR-18a was ectopically elevated in hMECs cultured on a soft ECM (Fig. 3h). We also observed an increase in Hoxa9 mRNA expression in PyMT tumors in which miR-18a had been knocked down and PTEN was restored, as well as a reduction in Hoxa9 mRNA expression in PyMT tumors in which miR-18a abundance had been increased and PTEN levels reduced (Fig. 3i,j). These findings imply a coordinate regulation of HOXA9 and PTEN by miR-18a, suggesting that ECM stiffness promotes malignancy by inducing miR-18a to reduce expression of HOXA9 and PTEN.

### ECM stiffness prevents HOXA9-dependent PTEN transcription

Our previously published microarray results suggested that HOXA9 induces PTEN expression in breast cancer cells<sup>24</sup>. Consistent with this predicted link between HOXA9 and PTEN, we noted that shRNA-mediated reduction of HOXA9 levels resulted in a significant loss of PTEN mRNA, even when nonmalignant hMECs were grown on a soft ECM where PTEN levels are elevated (Fig. 4a). Furthermore, increasing levels of HOXA9 using an expression plasmid lacking the HOXA9 3' UTR restored PTEN levels in nonmalignant hMECs grown on a stiff ECM and increased PTEN mRNA levels in two breast cancer cell lines (Fig. 4b,c). Moreover, ectopic expression of Hoxa9 in PyMT tumor cells orthotopically injected into FVB mice increased Pten mRNA expression and reduced growth and final tumor volume without affecting miR-18a levels (Fig. 4d-f). These findings indicate that HOXA9 modulates mammary tumorigenesis by regulating PTEN.

Reporter assays using the proximal promoter region of PTEN<sup>25,26</sup>, which contains homeobox consensus binding sites, confirmed that luciferase activity was enhanced after transfection with increasing amounts of a plasmid encoding WT HOXA9 but not after transfection with a DNA-binding domain-mutant HOXA9 (N255T; DNA BM) or with HOXA10 (Fig. 4g,h). These assays also confirmed that HOXA9 induces PTEN expression independent of the HOX cofactors PBX1 and MEIS1 (Fig. 4i). Chromatin immunoprecipitation (ChIP) studies conducted using endogenous HOXA9 as the bait (in MECs grown on soft ECMs where they express high levels of HOXA9 protein) confirmed that HOXA9 directly binds to the PTEN promoter (Fig. 4j). This effect was markedly decreased when HOXA9 levels were reduced

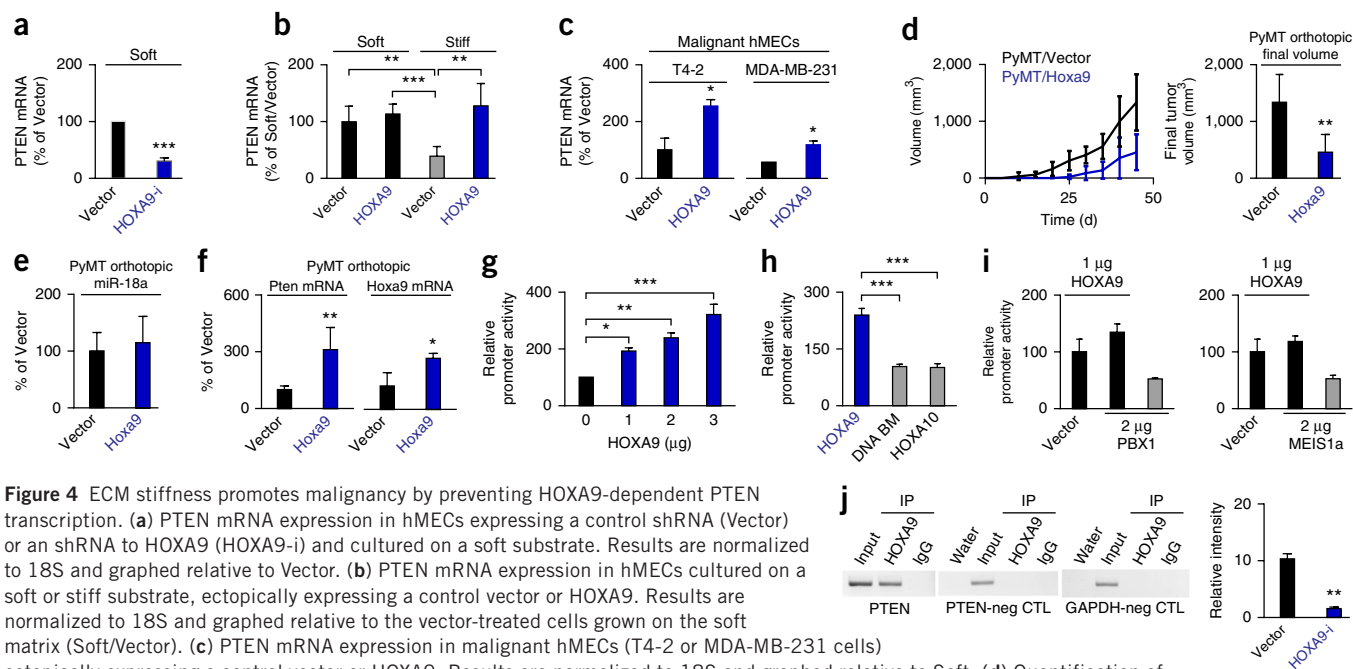


**Figure 4** ECM stiffness promotes malignancy by preventing HOXA9-dependent PTEN transcription. (a) PTEN mRNA expression in hMECs expressing a control shRNA (Vector) or an shRNA to HOXA9 (HOXA9-i) and cultured on a soft substrate. Results are normalized to 18S and graphed relative to Vector. (b) PTEN mRNA expression in hMECs cultured on a soft or stiff substrate, ectopically expressing a control vector or HOXA9. Results are normalized to 18S and graphed relative to the vector-treated cells grown on the soft matrix (Soft/Vector). (c) PTEN mRNA expression in malignant hMECs (T4-2 or MDA-MB-231 cells) ectopically expressing a control vector or HOXA9. Results are normalized to 18S and graphed relative to Soft. (d) Quantification of tumor growth and final tumor volume for PyMT primary tumor cells expressing either a control vector or Hoxa9 and orthotopically injected into the inguinal mammary gland of FVB hosts ( $n = 5$  per group). (e) miR-18a expression for orthotopic PyMT tumors expressing either a control vector or Hoxa9 ( $n = 5$  per group). Results are normalized to 18S and graphed relative to Vector. (f) Pten and Hoxa9 expression for orthotopic PyMT tumors expressing either a control vector or Hoxa9 ( $n = 5$  per group). Results are normalized to 18S and graphed relative to Vector. (g) Luciferase reporter analysis of PTEN promoter activity in response to the addition of WT HOXA9. (h) Luciferase reporter analysis of PTEN promoter activity upon addition of 2  $\mu$ g HOXA9 containing an N255T (DNA BM) mutation in the conserved DNA binding domain or the addition of 2  $\mu$ g of HOXA10. (i) Luciferase reporter analysis of PTEN promoter activity in response to 1  $\mu$ g HOXA9 with 2  $\mu$ g of either PBX1 or MEIS1a. (j) Representative gel of ChIP studies in hMECs revealing coprecipitation of HOXA9 with the PTEN promoter. Quantification of the chromatin immunoprecipitation results of HOXA9 on the PTEN proximal promoter for nonmalignant hMECs expressing either an shRNA control or an shRNA to HOXA9. Neg, negative. In all *in vitro* bar graphs, results are the mean  $\pm$  s.e.m. of at least 3 independent experiments. For *in vivo* bar graphs, results are the mean  $\pm$  s.d. (\* $P < 0.05$ ; \*\* $P < 0.01$ ; \*\*\* $P < 0.001$ ).

via shRNA (Fig. 4j). These findings indicate that HOXA9 directly binds to the PTEN promoter to regulate its expression and inhibit malignancy of breast cells. These results also demonstrate that increasing mechanical stiffness represses PTEN expression both directly via miR-18a targeting and indirectly via miR-18a targeting of HOXA9.

### Tissue stiffness engages mechanotransduction signaling

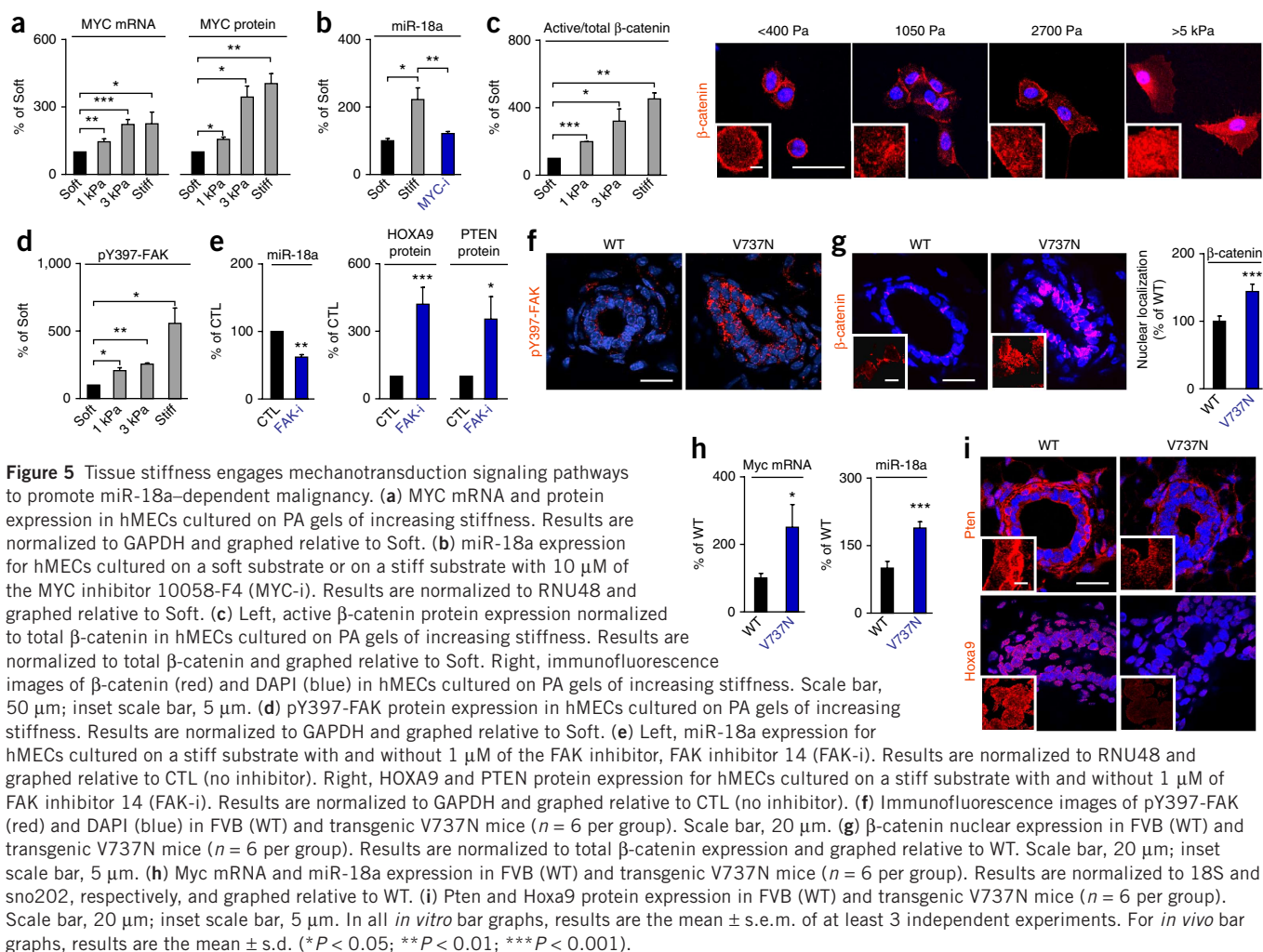
miRNAs exhibit differential expression across breast cancer subtypes<sup>27</sup>, with both tumor initiation and progression regulated by MYC proto-oncogene stimulation of the miR-17-92 cluster<sup>28</sup>. We therefore hypothesized that MYC-driven miRNA expression could be distinctly controlled by the mechanical microenvironment. Both mRNA and protein levels of MYC increased with substrate stiffness for nonmalignant and malignant hMECs (Fig. 5a and Supplementary Fig. 4a). Pharmacological inhibition of MYC in hMECs cultured on a stiff substrate reduced miR-18a levels (Fig. 5b), suggesting a functional link between MYC expression and mechanics. Myc mRNA expression was increased in mouse mammary tumors compared to WT glands, and LOX inhibition reduced both mRNA and protein expression relative to untreated tumors (Supplementary Fig. 4b), despite similar levels of cell proliferation (Supplementary Figs. 1c and 2f,g). These results suggest that MYC is upregulated by increasing matrix stiffness in culture and *in vivo*, at both the mRNA and protein levels.

Previous work established MYC as a downstream target of  $\beta$ -catenin signaling<sup>29</sup>. Nuclear  $\beta$ -catenin levels were increased in hMECs grown on stiff substrates (Supplementary Fig. 4c), and the ratio of activated to total  $\beta$ -catenin protein increased with substrate

stiffness (Fig. 5c and Supplementary Fig. 4c). Immunofluorescence also revealed that ECM stiffness increased total nuclear  $\beta$ -catenin (Fig. 5c). Moreover, nuclear localization of total  $\beta$ -catenin and  $\beta$ -catenin activation were reduced in glands with LOX-inhibited relative to control PyMT tumors (Supplementary Fig. 4d,e).

In both the culture and *in vivo* models,  $\beta$ -catenin mRNA levels were unchanged by ECM stiffness (Supplementary Fig. 4f). However, Y397-FAK phosphorylation (indicating FAK activation), glycogen synthase kinase-3 $\alpha$  (GSK-3 $\alpha$ ) and GSK-3 $\beta$  (GSK-3 $\alpha/\beta$ ) phosphorylation (indicating GSK-3 inactivation) and S473-Akt phosphorylation (indicating Akt activity) increased with stiffness, suggesting that integrin-dependent signaling activates  $\beta$ -catenin (Fig. 5d and Supplementary Figs. 2g and 5a,b). Inhibiting FAK reduced miR-18a expression and increased HOXA9 and PTEN protein expression (Fig. 5e). Additionally, inhibition of miR-18a reduced both Akt and GSK-3 $\alpha/\beta$  phosphorylation in hMECs cultured on stiff substrates (Supplementary Fig. 5c,d). These data demonstrate that tissue stiffening modulates miRNA-dependent PTEN expression through integrin-dependent activation of  $\beta$ -catenin and MYC.

To facilitate integrin clustering *in vivo*, transgenic mice expressing a conditional V737N  $\beta_1$  integrin clustering mutant, which recapitulates tension-dependent integrin clustering and promotes focal adhesion signaling<sup>2</sup>, were bred with transgenic mouse line expressing MMTV-Cre (Cre under control of mouse mammary tumor virus promoter) to promote mammary gland-specific expression. Consistent with enhancement of focal adhesion assembly and signaling, Y397-FAK phosphorylation increased in the V737N mutant glands (Fig. 5f).



$\beta$ -catenin nuclear localization was also increased in the epithelium of the V737N mammary glands (Fig. 5g), as were Myc mRNA and miR-18a levels (Fig. 5h). Notably, Hoxa9 mRNA and protein expressions were inversely correlated with miR-18a in normal and V737N mutant mammary glands (Fig. 5i and Supplementary Fig. 5e). Finally, Pten mRNA and protein expression levels were reduced in the V737N mammary glands compared to in WT controls (Fig. 5i and Supplementary Fig. 5f). These results indicate that the mechanical microenvironment influences PTEN expression downstream of integrin activation of  $\beta$ -catenin signaling.

### Breast malignancy associates with increased miR-18a

We investigated the clinical relevance of ECM stiffness-induced miR-18a upregulation and PTEN repression by assessing the RNA and protein expression of HOXA9 and PTEN in cohorts of clinically diverse human breast cancers and normal tissue. miR-18a expression was notably higher in samples from patients with breast cancer than in nonmalignant samples, with expression in either basal-like or luminal B samples significantly higher than the expression in either the normal or luminal A samples (Fig. 6a). As measured by atomic force microscopy, miR-18a expression correlated with breast ECM stiffness in both normal and transformed breast tissue ( $R^2 = 0.7197$ ,  $P < 0.001$ , Fig. 6b), with luminal B samples stiffer than luminal A samples (Fig. 6c). PTEN and HOXA9 mRNA expressions were reduced in

luminal B cancers compared to normal breast tissue, and further reduced in basal-like cancers (Fig. 6d). Indeed, HOXA9 correlated with PTEN in normal and transformed breast tissue for both mRNA ( $R^2 = 0.8979$ ) and protein expressions, consistent with our findings that PTEN is regulated by HOXA9 (Fig. 6e,f). The epithelium of normal breast tissue coexpressed appreciable quantities of nuclear HOXA9 and cytoplasmic PTEN proteins, as did the more differentiated luminal A breast tumors (Fig. 6f). In contrast, the less differentiated luminal B, basal-like and HER2<sup>+</sup> tumors showed reduced expression of HOXA9 and PTEN and higher levels of activated AKT (pAKT substrate), phospho-S6 and inactivated pGSK-3 (Fig. 6f and Supplementary Fig. 6a). These clinical findings, together with our experimental data, are consistent with the notion that miR-18a and HOXA9 modulate PTEN expression by cooperating with multiple negative and positive regulatory factors differentially expressed in human breast tumors<sup>13</sup>.

We next analyzed publicly available gene expression data sets to look for associations between miR-18a and clinical outcome<sup>30,31</sup>. In patient samples without mutations in PTEN, we found that the expression of PTEN correlated with miR-18a expression, but only if HOXA9 was unmethylated ( $P < 0.0001$ , Supplementary Fig. 6b). We found that miR-18a expression inversely correlated with time to distant relapse-free survival (DRFS) in patients whose tumors expressed the highest miR-18a levels at initial diagnosis (highest quartile) and experienced

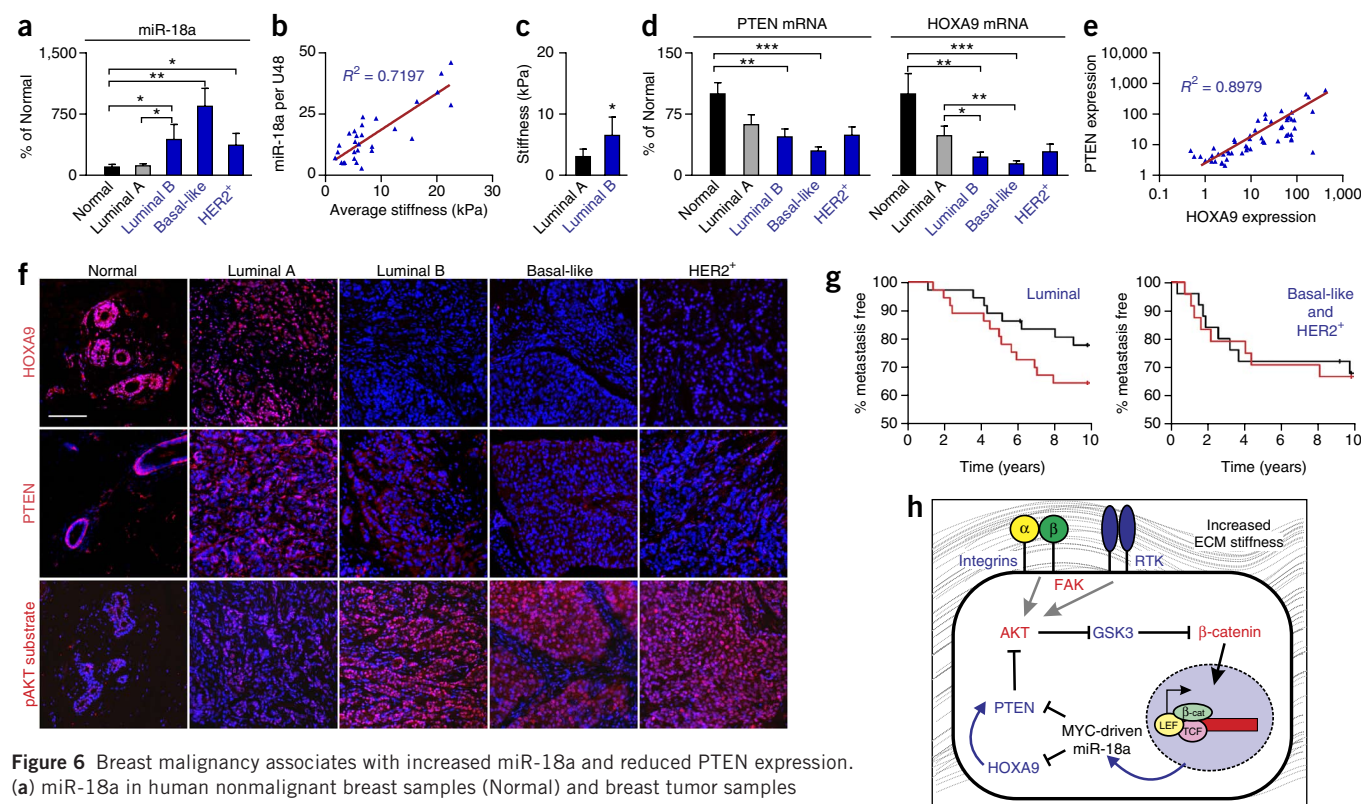


**Figure 6** Breast malignancy associates with increased miR-18a and reduced PTEN expression. (a) miR-18a in human nonmalignant breast samples (Normal) and breast tumor samples (luminal A, luminal B, basal-like and HER2<sup>+</sup>). Results are normalized to RNU48 and graphed relative to Normal. (b) Correlation between miR-18a expression and elastic modulus (upper quartile) in human patient samples (both nonmalignant and tumor samples combined). (c) Elastic moduli (upper quartile) for luminal A and luminal B breast tumor samples. (d) PTEN and HOXA9 mRNA expression in human nonmalignant breast samples and breast tumor samples. Results are normalized to 18S and graphed relative to Normal. (e) Correlation between HOXA9 and PTEN mRNA levels in human patient samples (both nonmalignant and tumor samples combined). (f) HOXA9 (top, red), PTEN (middle, red), pAKT substrate (bottom, red) and DAPI (blue) for human nonmalignant breast samples and breast tumor samples. Scale bar, 100  $\mu$ m. (g) Left, Kaplan-Meier graph showing that patients with luminal breast cancers whose tumors expressed the highest miR-18a levels (highest expression quartile, red line) experienced significantly reduced metastasis-free survival compared with patients in the lowest quartile (black line). Right, Kaplan-Meier graph showing patients with basal-like and HER2<sup>+</sup> breast cancers whose tumors expressed the highest miR-18a levels (highest expression quartile; red line) and lowest miR-18a levels (black line). (h) Graphic depicting a model for suppression of PTEN directly via  $\beta$ -catenin stimulation of MYC-driven miR-18a and indirectly through miR-18a regulation of HOXA9. RTK, receptor tyrosine kinase; LEF, lymphoid enhancer-binding factor; TCF, T cell factor. \* $P < 0.05$ ; \*\* $P < 0.01$ ; \*\*\* $P < 0.001$ .

distant metastases as a second event, regardless of subtype ( $P = 0.0173$ , **Supplementary Fig. 6c**). Including multiple PTEN-targeting miRNAs in two different models, we found that miR-18a expression levels were predictive of outcome among patients with luminal breast cancers ( $P = 0.017$  and  $P = 0.049$ , **Fig. 6g** and **Supplementary Fig. 6d**). These data indicate that miR-18a is upregulated in basal-like breast cancers and its expression correlates with increased future disease aggression for patients with luminal breast cancers. Combined, these findings identify a mechanically regulated molecular circuit that may promote malignancy and suggest that matrix stiffness could influence breast cancer pathogenesis (**Fig. 6h**).

## DISCUSSION

Here, we demonstrate that miRNA expression is responsive to ECM stiffness. We present *in vitro* and *in vivo* evidence to show that one miRNA, miR-18a, mediates stiffness-dependent malignancy of breast epithelium. By demonstrating that elevated ECM stiffness engages a miR-18a circuit that promotes PI3K-dependent malignant progression by targeting the tumor suppressor PTEN directly and indirectly via tumor modifier HOXA9, we established miRNAs as key mediators of tumor mechanics. Given that tissue mechanics are often altered in tumors, our findings provide a plausible explanation for the frequent

alteration of miRNA expression across multiple cancer types<sup>6</sup>. Indeed, integrin adhesions and ion channel activity are central players in mechanotransduction that are altered in malignancy and regulated by miRNAs<sup>7,32,33</sup>. Notably, ECM stiffness is one of multiple aspects of tissue mechanics, which also compromises tissue architecture, interstitial pressure and mass transport; these physical cues also influence miRNA expression, thereby reinforcing the concept that miRNAs are part of a force-regulated signaling network<sup>1,34–36</sup>.

Ultrasound and shear wave elastography interrogate tissue stiffness as a screening procedure to detect cancer<sup>37–39</sup>. Yet, studies in experimental models argue that tissue mechanics have more than just a passenger role in tumor progression<sup>2,3,34</sup>. In patient biopsies, our data indicate that miR-18a levels can distinguish luminal A from luminal B tumors and predict clinical outcome in patients with luminal type breast cancer. Our studies are consistent with elastography data on patients with breast cancer, suggesting that macro-level tumor stiffness may parallel aggression, with tumor size, grade and subtype as independent factors influencing tissue mechanics<sup>38–40</sup>. We extend these observations to show that ECM stiffness can engage a specific molecular pathway, miR-18a regulation of PTEN and HOXA9, that could be clinically exploited. In this regard, luminal breast cancers vary heterogeneously in terms of gene expression, mutations, copy

number changes and patient outcome and present a major challenge to identify patients with aggressive versus indolent tumors<sup>31,41,42</sup>. Our work identifies ECM stiffness as a biophysical parameter that can distinguish luminal A from luminal B tumors with miR-18a, PTEN and HOXA9 presenting as tractable biomarkers.

## METHODS

Methods and any associated references are available in the [online version of the paper](#).

*Note: Any Supplementary Information and Source Data files are available in the online version of the paper.*

## ACKNOWLEDGMENTS

We thank the members of the Weaver and N. Boudreau labs for helpful discussions. Atomic force microscopy analysis of the PyMT samples was performed by H. Yu. Animal handling was supported by L. Korets. miRNA and antagomir constructs were provided by M. Scherr at the Medical School Hannover. PTEN proximal promoter constructs were provided by C. Eng at the Genomic Medical Institute. LOX inhibitory antibodies were provided by A. Giaccia at the Stanford University School of Medicine. HOXA9 was provided by T. Nakamura at the Japanese Foundation for Cancer Research. This work was supported by US Department of Defense Breast Cancer Research Program (DOD BCRP) grant W81XWH-07-1-0538 (J.K.M.), Susan G. Komen Postdoctoral Fellowship PDF12230246 (I.A.), US National Science Foundation Graduate Research Fellowship (G.O.), DOD BCRP grants W81XWH-05-1-0330 and W81XWH-13-1-0216 (V.M.W.), US National Institutes of Health NCI grants R01 CA138818, U54 CA143836, R01 CA085492 and U01 ES019458 (V.M.W.) and Susan G. Komen grant KG110560PP (V.M.W. and E.S.W.).

## AUTHOR CONTRIBUTIONS

J.K.M., Y.Y. and L.D. conducted PyMT and V737N mouse experiments. J.K.M., A.C.W. and K.R.L. fabricated and conducted experiments with the PA hydrogels. R.O.B. and J.K.M. performed the miRNA and large-scale gene expression analyses. J.N.L. designed and constructed expression constructs and the V737N transgenic mouse. J.K.M. and Y.Y. performed immunofluorescence imaging, and G.O. performed the ImageJ analyses. I.A. performed AFM measurements. E.S.H. collected the human patient samples and aided in the interpretation of the data. Y.-Y.C. aided with pathological breast cancer subtyping. P.M.G. conducted the HOXA9 microarray analysis<sup>25</sup>. V.M.W. and J.K.M. wrote the manuscript with input from all authors.

## COMPETING FINANCIAL INTERESTS

The authors declare no competing financial interests.

Reprints and permissions information is available online at <http://www.nature.com/reprints/index.html>.

- Kumar, S. & Weaver, V.M. Mechanics, malignancy, and metastasis: the force journey of a tumor cell. *Cancer Metastasis Rev.* **28**, 113–127 (2009).
- Paszek, M.J. *et al.* Tensional homeostasis and the malignant phenotype. *Cancer Cell* **8**, 241–254 (2005).
- Levental, K.R. *et al.* Matrix crosslinking forces tumor progression by enhancing integrin signaling. *Cell* **139**, 891–906 (2009).
- Provenzano, P.P. *et al.* Enzymatic targeting of the stroma ablates physical barriers to treatment of pancreatic ductal adenocarcinoma. *Cancer Cell* **21**, 418–429 (2012).
- Tavazoie, S.F. *et al.* Endogenous human microRNAs that suppress breast cancer metastasis. *Nature* **451**, 147–152 (2008).
- Zhang, B., Pan, X., Cobb, G.P. & Anderson, T.A. microRNAs as oncogenes and tumor suppressors. *Dev. Biol.* **302**, 1–12 (2007).
- Valastyan, S. & Weinberg, R.A. Roles for microRNAs in the regulation of cell adhesion molecules. *J. Cell Sci.* **124**, 999–1006 (2011).
- Taylor, M.A., Sossey-Alaoui, K., Thompson, C.L., Danielpour, D. & Schieman, W.P. TGF- $\beta$  upregulates miR-181a expression to promote breast cancer metastasis. *J. Clin. Invest.* **123**, 150–163 (2013).

- Neth, P., Nazari-Jahantigh, M., Schober, A. & Weber, C. MicroRNAs in flow-dependent vascular remodelling. *Cardiovasc. Res.* **99**, 294–303 (2013).
- Yehya, N., Yerrapureddy, A., Tobias, J. & Margulies, S.S. MicroRNA modulate alveolar epithelial response to cyclic stretch. *BMC Genomics* **13**, 154 (2012).
- Krasilnikov, M.A. Phosphatidylinositol-3 kinase dependent pathways: the role in control of cell growth, survival, and malignant transformation. *Biochemistry (Mosc.)* **65**, 59–67 (2000).
- Hollander, M.C., Blumenthal, G.M. & Dennis, P.A. PTEN loss in the continuum of common cancers, rare syndromes and mouse models. *Nat. Rev. Cancer* **11**, 289–301 (2011).
- Salmena, L., Carracedo, A. & Pandolfi, P.P. Tenets of PTEN tumor suppression. *Cell* **133**, 403–414 (2008).
- Olive, V., Li, Q. & He, L. mir-17–92: a polycistronic oncomir with pleiotropic functions. *Immunol. Rev.* **253**, 158–166 (2013).
- Li, Y. *et al.* The miR-17–92 cluster expands multipotent hematopoietic progenitors whereas imbalanced expression of its individual oncogenic miRNAs promotes leukemia in mice. *Blood* **119**, 4486–4498 (2012).
- Suárez, Y. *et al.* Dicer-dependent endothelial microRNAs are necessary for postnatal angiogenesis. *Proc. Natl. Acad. Sci. USA* **105**, 14082–14087 (2008).
- Kenny, P.A. *et al.* The morphologies of breast cancer cell lines in three-dimensional assays correlate with their profiles of gene expression. *Mol. Oncol.* **1**, 84–96 (2007).
- Scherr, M. *et al.* Lentivirus-mediated antagomir expression for specific inhibition of miRNA function. *Nucleic Acids Res.* **35**, e149 (2007).
- John, B. *et al.* Human MicroRNA targets. *PLoS Biol.* **2**, e363 (2004).
- Betel, D., Koppal, A., Agius, P., Sander, C. & Leslie, C. Comprehensive modeling of microRNA targets predicts functional non-conserved and non-canonical sites. *Genome Biol.* **11**, R90 (2010).
- Betel, D., Wilson, M., Gabow, A., Marks, D.S. & Sander, C. The microRNA.org resource: targets and expression. *Nucleic Acids Res.* **36**, D149–D153 (2008).
- Enright, A.J. *et al.* MicroRNA targets in *Drosophila*. *Genome Biol.* **5**, R1 (2003).
- Jin, Y., Chen, Z., Liu, X. & Zhou, X. Evaluating the microRNA targeting sites by luciferase reporter gene assay. *Methods Mol. Biol.* **936**, 117–127 (2013).
- Gilbert, P.M. *et al.* HOXA9 regulates BRCA1 expression to modulate human breast tumor phenotype. *J. Clin. Invest.* **120**, 1535–1550 (2010).
- Moens, C.B. & Selleri, L. Hox cofactors in vertebrate development. *Dev. Biol.* **291**, 193–206 (2006).
- Tang, Y. & Eng, C. PTEN autoregulates its expression by stabilization of p53 in a phosphatase-independent manner. *Cancer Res.* **66**, 736–742 (2006).
- Vingge, H. *et al.* The shaping and functional consequences of the microRNA landscape in breast cancer. *Nature* **497**, 378–382 (2013).
- Dews, M. *et al.* Augmentation of tumor angiogenesis by a Myc-activated microRNA cluster. *Nat. Genet.* **38**, 1060–1065 (2006).
- He, T.C. *et al.* Identification of c-MYC as a target of the APC pathway. *Science (New York, N.Y.)* **281**, 1509–1512 (1998).
- Buffa, F.M. *et al.* microRNA-associated progression pathways and potential therapeutic targets identified by integrated mRNA and microRNA expression profiling in breast cancer. *Cancer Res.* **71**, 5635–5645 (2011).
- Cancer Genome Atlas Network. Comprehensive molecular portraits of human breast tumours. *Nature* **490**, 61–70 (2012).
- Delmas, P. & Coste, B. Mechano-gated ion channels in sensory systems. *Cell* **155**, 278–284 (2013).
- Wang, Z. miRNA in the regulation of ion channel/transporter expression. *Compr. Physiol.* **3**, 599–653 (2013).
- Provenzano, P.P., Inman, D.R., Eliceiri, K.W. & Keely, P.J. Matrix density-induced mechanoregulation of breast cell phenotype, signaling and gene expression through a FAK-ERK linkage. *Oncogene* **28**, 4326–4343 (2009).
- Huang, S. & Ingber, D.E. Cell tension, matrix mechanics, and cancer development. *Cancer Cell* **8**, 175–176 (2005).
- Vogel, V. & Sheetz, M. Local force and geometry sensing regulate cell functions. *Nat. Rev. Mol. Cell Biol.* **7**, 265–275 (2006).
- Fasching, P.A. *et al.* Influence of mammographic density on the diagnostic accuracy of tumor size assessment and association with breast cancer tumor characteristics. *Eur. J. Radiol.* **60**, 398–404 (2006).
- Chang, J.M. *et al.* Stiffness of tumours measured by shear-wave elastography correlated with subtypes of breast cancer. *Eur. Radiol.* **23**, 2450–2458 (2013).
- Evans, A. *et al.* Quantitative shear wave ultrasound elastography: initial experience in solid breast masses. *Breast Cancer Res.* **12**, R104 (2010).
- Chang, J.M. *et al.* Clinical application of shear wave elastography (SWE) in the diagnosis of benign and malignant breast diseases. *Breast Cancer Res. Treat.* **129**, 89–97 (2011).
- Paik, S. *et al.* A multigene assay to predict recurrence of tamoxifen-treated, node-negative breast cancer. *N. Engl. J. Med.* **351**, 2817–2826 (2004).
- Parker, J.S. *et al.* Supervised risk predictor of breast cancer based on intrinsic subtypes. *J. Clin. Oncol.* **27**, 1160–1167 (2009).

## ONLINE METHODS

**Antibodies and reagents.** Antibodies and reagents were as follows: Matrigel recombinant basement membrane (BD Biosciences), FAK inhibitor 14 (1  $\mu$ M, Tocris), NE-PER Nuclear and Cytoplasmic Extraction Kit (Thermo Scientific) and antibodies to PTEN (Cell Signaling 9559, 1:1,000), HOXA9 for immunofluorescence (a gift from T. Nakamura, 1:200), HOXA9 for western blotting (Santa Cruz sc-17155, 1:500), pS473-Akt (Cell Signaling 4060, 1:1,000 for western blot, 1:200 for immunofluorescence), phospho-Akt substrate (Cell Signaling 9614, 1:1,000), pan-Akt (Cell Signaling 4691, 1:1,000),  $\beta$ -actin (Sigma A228, 1:2,000), Gapdh (Cell Signaling 2118, 1:1,000), MYC (Abcam ab32072, 1:10,000), active  $\beta$ -catenin (Cell Signaling 8814, 1:1,000), total  $\beta$ -catenin (Cell Signaling 8480, 1:1,000 for western blotting, 1:100 for immunofluorescence), phospho-GSK-3 $\alpha$ / $\beta$  (Cell Signaling 9331, 1:1,000 for western blotting, 1:50 for immunofluorescence), GSK-3 $\alpha$ / $\beta$  (Cell Signaling 5676, 1:1,000), pY397-FAK (Invitrogen 44625, 1:500 for western blotting, 1:200 for immunofluorescence), phospho-histone H3 (Cell Signaling 9701, 1:1,000), cleaved caspase-3 (Cell Signaling 9661, 1:1,000 for western blotting, 1:400 for immunofluorescence) and phospho-S6 (Cell Signaling 2211, 1:1,000 for western blotting, 1:200 for immunofluorescence) and AlexaFluor-conjugated goat secondary anti-mouse IgG and anti-rabbit IgG antibodies (Invitrogen A11012, 1:1,000; Invitrogen A11005, 1:1,000).

**Polyacrylamide substrates and cell manipulations.** The HMT-3522 S-1 and T4-2 MECs were grown and manipulated as described previously<sup>43,44</sup>. MCF-10A, MCF-7 and MDA-MB-231 cells were cultured according to manufacturer's recommendations (ATCC)<sup>2</sup>. Basement membrane-conjugated polyacrylamide hydrogels were prepared as previously described<sup>45</sup> with one modification: *n*-succinimidyl acrylamidohexanoic acid crosslinker was conjugated to polyacrylamide substrates using 0.01% bisacrylamide, 0.025% Irgacure 2959 0.002% Di(trimethylolpropane) tetracrylate (Sigma) and 0.01% *n*-succinimidyl acrylamidohexanoic acid. Soft agar assays were performed as previously described<sup>24</sup>.

**Vector constructs and gene expression.** miR-18a, antagomir to miR-18a and antagomir to miR-19b constructs, as well as miRNA and antagomir control constructs, have been previously described<sup>18,46</sup>. shRNA constructs targeting HOXA9 have been previously described<sup>24</sup>. HOXA9 was PCR amplified from our previously described HOXA9 retroviral vector<sup>24</sup> and inserted into the pLV vector to generate the HOXA9 lentiviral expression vector using a previously described approach<sup>47</sup>.

**Mice and treatments.** All mice were maintained in accordance with University of California Institutional Animal Care and Use Committee guidelines. For LOX inhibition studies, FVB/NJ and FVB/N-Tg(MMTV-PyVT) mice (The Jackson Laboratory) were treated with BAPN (3 mg per kg body weight; Spectrum) in the drinking water ( $n = 10$  per group) or a LOX function-blocking polyclonal antibody (3 mg per kg body weight; OpenBiosystems, D8746) injected intraperitoneally twice per week ( $n = 5$  per group). Treatment started at 4 weeks and mice were killed after 11 weeks. Lesions were detected by palpation, and tumor volume was assessed with calipers. To generate the FVB/N-Tg (MMTV-V737N) mice, the V737N mutation of the  $\beta 1$  integrin was cloned downstream of a floxed neomycin phosphotransferase expression cassette in a ROSA26 targeting construct. Transgenic mice expressing the conditional V737N integrin  $\beta 1$  clustering mutant were bred with the mammary gland-specific MMTV-Cre transgenic mice to generate the FVB/N-Tg (MMTV-V737N) mice (age, 6 weeks;  $n = 6$  per group). After the mice were killed, mammary glands were excised, imaged and snap frozen or fixed with paraformaldehyde.

For orthotopic injection studies, primary PyMT tumor cells were isolated from PyMT tumors (from 11-week-old mice).  $1 \times 10^6$  primary cells ectopically expressing miR-18a ( $n = 6$  per group), an antagomir to miR-18a (ant-18a,  $n = 5$  per group), Hoxa9 ( $n = 5$  per group) or respective appropriate controls were injected into inguinal mammary fat pads of 6- to 7-week-old host FVB mice. Mice were killed when tumors reached 1–2 cm. Lesions were detected by palpation, and tumor volume was assessed with calipers. After killing the mice, tumors were excised, imaged and snap frozen or fixed with paraformaldehyde. When relevant, metastatic burden was assessed by qPCR for PyMT. For tail vein studies, primary PyMT tumor cells were isolated from PyMT tumors (from 11-week-old mice).

$5 \times 10^5$  primary cells ectopically expressing an antagomir to miR-18a (ant-18a) or an antagomir control (ant-CTL) were suspended in PBS and injected into the tail veins of 6- to 7-week-old host FVB mice ( $n = 6$  per group). Mice were killed after 28 d. Metastatic burden was assessed by wet lung weight.

**miRNA arrays and quantitative PCR.** Affymetrix miRNA labeling, array hybridization and data preprocessing were performed as previously described<sup>48</sup>. For hMECs microarray experiments, two to four independent experiments were performed under identical conditions. For *in vivo* microarray experiments,  $n = 4$  independent mammary glands (inguinal) per group. Data were extracted from the images, quantile-normalized, summarized (median polish) and log<sub>2</sub>-transformed with the miRNA QC tool software from Affymetrix. For miRNA qPCR analysis, reverse transcription of specific miRNAs (from 10 ng of total RNA) was carried out using the real-time loop primers for each type of miRNA and the TaqMan miRNA RT Kit from Applied Biosystems, according to instructions. cDNA obtained from this step was used to do real-time quantitative TaqMan PCR using the real-time primers provided, according to instructions. Ct values were converted to fold expression changes ( $2^{-\Delta\Delta Ct}$  values) following normalization to U6 small nuclear RNA, RNU48 or sno202. For the identification of target miRNAs, attention was focused on miRNAs upregulated in hMECs cultured in a stiff microenvironment, upregulated in the mammary glands of PyMT mice (compared to nonmalignant FVB mammary glands) and reduced in LOX-inhibited PyMT mammary glands (compared to control PyMT glands). Additionally, previous work suggests that the most abundant miRNAs in a cell mediate target suppression<sup>49</sup>. miRNA abundance was estimated in the microarray analyses as presented in **Supplementary Tables 1–4**.

For mRNA analysis, total RNA was reverse-transcribed using random primers (Amersham Biosciences), and GAPDH or 18S primers were used to control for cDNA concentration in a separate PCR reactions for each sample. LightCycler Fast Start DNA Master SYBR Green Mix (Roche) was added to each PCR reaction along with cDNA and 1 pmol primer in a total volume of 10  $\mu$ l.

**Atomic force microscopy.** Atomic force microscopy and analysis were performed using an MFP3D-BIO inverted optical atomic force microscope mounted on a Nikon TE2000-U inverted fluorescent microscope (Asylum Research) as previously described<sup>50</sup>.

**Immunostaining, immunoblotting, chromatin immunoprecipitation and reporter assays.** Immunofluorescence imaging of cultures and tissues was performed as described<sup>2</sup>. Cells were lysed in RIPA or Laemmli buffer and assayed by immunoblotting<sup>51</sup>. ChIP assays were performed as previously described<sup>25</sup>. Luciferase reporter assays were quantified by SEAP expression and were performed as previously described<sup>23,24</sup>. For the V737N  $\beta$ -catenin nuclear localization analysis shown in **Figure 5g**,  $\beta$ -catenin and DAPI colocalization was determined via ImageJ, and non-nuclear  $\beta$ -catenin has been removed from the images displayed. Picrosirius red analysis was performed on paraffin sections of mammary glands, and tumors were stained with 0.1% picrosirius red (Sigma) and counterstained with Weigert's hematoxylin to reveal fibrillar collagen. Sections were imaged using an Olympus IX81 fluorescence microscope fitted with an analyzer (U-ANT) and polarizer (U-POT, Olympus) oriented parallel and orthogonal to each other.

**Human samples.** Breast cancer subtypes were approximated using defined clinicopathological criteria<sup>52,53</sup>. Briefly, luminal A tumors are defined as ER and/or PR positive, HER2 negative and Ki-67 low (<14%); luminal B tumors are defined as ER and/or PR positive, HER2 negative and Ki-67 high (or any Ki-67 status and HER2 amplified); basal-like tumors are defined as ER and PR negative, with HER2 not overexpressed or amplified; and HER2-overexpressing tumors are defined as ER and PR negative, with HER2 overexpressed or amplified.

Formalin-fixed, paraffin-embedded human breast tissue sections and freshly isolated RNA, lacking any patient-identifying information, were obtained with institutional review board (IRB) approval (NCoR2, Breast Tumor Metastasis and Treatment Resistance, IRB 10-05046 and Collagen Remodeling and Tumor Progression, IRB 10-03832) from the University of California, San Francisco, with written patient consent or commercially (Biomax or OriGene). Immunofluorescence was performed as previously described<sup>24</sup>. For miRNA and

mRNA assays, 15 nonmalignant, 25 luminal A, 25 luminal B, 25 basal-like and 15 HER2<sup>+</sup> samples were examined. For analyses of paraffin-embedded sections, 10 nonmalignant, 20 luminal A, 20 luminal B, 20 basal-like and 35 HER2<sup>+</sup> samples were examined.

**Bioinformatics.** We related the expression of miR-18a to DRFS in a panel of breast cancers by fitting a multivariate Cox regression model to the data<sup>30,31</sup>. In the model, we stratified patients by subtype<sup>52,53</sup> and included independent covariates modeling miR-18a expression, patient age and tumor size, as well as the abundance of PTEN-regulating miRNAs including miR-222, miR-32, miR-26a, miR-106b, miR-25 and miR-93 as continuous variables. We included tumor grade and lymph node positivity as binary factors. We estimated the significance of the association of each covariate to DRFS in the framework of the regression model using a Wald test to generate *P* values. We visualized patient survival within each subgroup as Kaplan-Meier curves by plotting the surviving proportion of patients within the top and bottom quartiles of miR-18a expression as a function of time. To generate the heatmap images, we estimated the correlation between mRNA and miRNA abundance and patient outcome by calculating pairwise Spearman correlation coefficients between the normalized expression estimates or untransformed DRFS values across all patients as appropriate and clustered the resulting correlation matrices by Euclidean distance.

To examine the relationship between miR-18a and PTEN when HOXA9 is either methylated or unmethylated, graphs comparing PTEN expression to miR-18a expression were generated using all samples for which methylation data, miRNA expression estimates and mRNA expression estimates are available in The Cancer Genome Atlas breast cancer cohort<sup>31</sup>. Samples from the upper (methylated) and lower (unmethylated) quartiles of the relative methylation probe intensity levels for HOXA9 were plotted separately. The *x* and *y* axes indicate the normalized expression estimates for each sample, and a least-squares linear fit trendline is indicated in red (**Supplementary Fig. 6b**).

**Statistical analyses.** Statistical analyses were performed with an unpaired Student's *t*-test, two-way analysis of variance, general linear model, Fisher's exact test or Mann-Whitney *U*-test (where appropriate). Expression estimates represented in violin plots were analyzed with a Kolmogorov-Smirnov test. We used Minitab software to conduct the statistical analysis of our data. *P* values of less than 0.05 were considered to be significant.

43. Wang, F. *et al.* Reciprocal interactions between  $\beta_1$ -integrin and epidermal growth factor receptor in three-dimensional basement membrane breast cultures: a different perspective in epithelial biology. *Proc. Natl. Acad. Sci. USA* **95**, 14821–14826 (1998).
44. Weaver, V.M. *et al.* Reversion of the malignant phenotype of human breast cells in three-dimensional culture and *in vivo* by integrin blocking antibodies. *J. Cell Biol.* **137**, 231–245 (1997).
45. Lakins, J.N., Chin, A.R. & Weaver, V.M. Exploring the link between human embryonic stem cell organization and fate using tension-calibrated extracellular matrix functionalized polyacrylamide gels. *Methods Mol. Biol.* **916**, 317–350 (2012).
46. Stegmeier, F., Hu, G., Rickles, R.J., Hannon, G.J. & Elledge, S.J. A lentiviral microRNA-based system for single-copy polymerase II-regulated RNA interference in mammalian cells. *Proc. Natl. Acad. Sci. USA* **102**, 13212–13217 (2005).
47. Paszek, M.J. *et al.* Scanning angle interference microscopy reveals cell dynamics at the nanoscale. *Nat. Methods* **9**, 825–827 (2012).
48. Gan, L., Schwengberg, S. & Denecke, B. MicroRNA profiling during cardiomyocyte-specific differentiation of murine embryonic stem cells based on two different miRNA array platforms. *PLoS ONE* **6**, e25809 (2011).
49. Mullokandov, G. *et al.* High-throughput assessment of microRNA activity and function using microRNA sensor and decoy libraries. *Nat. Methods* **9**, 840–846 (2012).
50. Lopez, J.I., Mouw, J.K. & Weaver, V.M. Biomechanical regulation of cell orientation and fate. *Oncogene* **27**, 6981–6993 (2008).
51. Johnson, K.R., Leight, J.L. & Weaver, V.M. Demystifying the effects of a three-dimensional microenvironment in tissue morphogenesis. *Methods Cell Biol.* **83**, 547–583 (2007).
52. Goldhirsch, A. *et al.* Strategies for subtypes—dealing with the diversity of breast cancer: highlights of the St. Gallen International Expert Consensus on the Primary Therapy of Early Breast Cancer 2011. *Ann. Oncol.* **22**, 1736–1747 (2011).
53. Von Minckwitz, G. *et al.* Response-guided neoadjuvant chemotherapy for breast cancer. *J. Clin. Oncol.* **31**, 3623–3630 (2013).